THE JOURNAL OF PHYSICAL CHEMISTRY LETTERS
A JOURNAL OF THE AMERICAN CHEMICAL SOCIETY

pubs.acs.org/JPCL Letter

Kinetic Superselectivity in Multivalent Binding

Vid Ravnik, Baptiste Chabaud, Urban Bren, Galina V. Dubacheva,* and Tine Curk*

Cite This: J. Phys. Chem. Lett. 2026, 17, 6357−6364 Read Online

ACCESS | Metrics & More | Article Recommendations | Supporting Information

ABSTRACT: Multivalent binding employs multiple simultaneous supramolecular interactions, increasing avidity and selectivity compared with monovalent binding. While equilibrium aspects of multivalency are well characterized, nonequilibrium behavior remains poorly understood. By combining experiments on hyaluronic acid polymers with kinetic modeling based on stochastic chemical kinetics and molecular dynamics simulations, we systematically investigate the kinetics of multivalent binding. Notably, we find that both association and dissociation kinetics can be more selective than equilibrium binding. We explain this behavior using a two-step binding model featuring a combination of fast, weak and slow, strong interactions. These findings demonstrate a new approach: superselective targeting based on the association rate instead of the equilibrium state. The kinetic theory and experiments presented here provide a fundamental understanding of multivalent kinetics and establish design rules for superselective targeting in out-of-equilibrium systems.

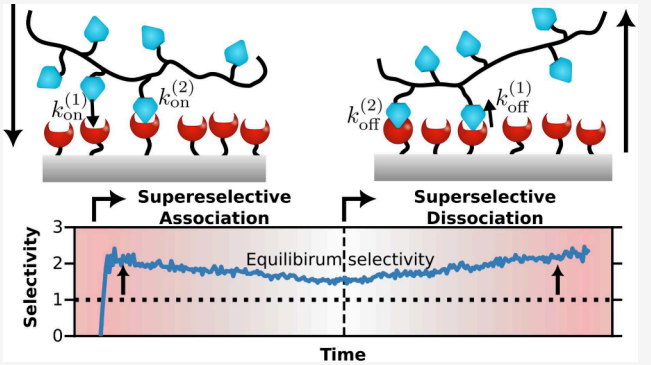

Multivalency is characterized by the simultaneous interaction of multiple binding partners.[1] While multivalent interactions result in increased binding strength (avidity) as compared to their monovalent counterparts, a more interesting consequence is superselectivity.[2] Due to the combinatorial entropy of multiple bound states, multivalent binders can sharply discriminate between surfaces based on their receptor concentration or other control parameters, facilitating supramolecular recognition and selective targeting applications.[3−7]

The thermodynamics of multivalent binding has been the subject of numerous theoretical and experimental studies,[2,7−11] and the design principles for multivalent superselectivity in equilibrium are well understood. However, practical synthetic and biological systems often rely on transient encounters under transport and turnover constraints, so the relevant question is not only how a multivalent entity binds at equilibrium, but also how selectively it accumulates, persists, or is cleared. Kinetic selectivity may thus be critical for processes such as cell (pathogen) adhesion and communication[12−15] and immune recognition,[16−18] where early binding events can trigger downstream responses. Understanding kinetic selectivity can also guide the design of biosensors or multivalent therapeutics that must achieve rapid and selective capture in complex environments, while avoiding off-target binding.[19−22]

Experimental investigations of multivalent kinetics[23,24] have consistently demonstrated that increased avidity observed in multivalent binding is primarily due to decreased dissociation rates.[14,25−29] However, existing kinetic models explore at most trivalent interactions[26,30−33] and do not explore superselective binding. Our goal is to understand the kinetic response of multivalent interactions and predict selectivity during the association and dissociation processes. To this end, we develop a theoretical model of multivalent binding kinetics and compare its predictions to a well-defined experimental platform based on host−guest interactions between hyaluronic acid (HA) substituted with β-cyclodextrin (β-CD) ligands[7,34] and self-assembled monolayers (SAMs) functionalized with ferrocene (Fc). We further validate the kinetic model with molecular dynamics (MD) simulations.

Using the experimental model system (Figure 1A), we investigate the kinetic response upon injection of multivalent polymers to surfaces with tunable receptor (Fc) densities Γ_{rec}. The surface chemistry and synthetic protocols for Fc SAM formation and HA functionalization with β-CD ligands are described in our previous studies[34,35] and Supporting Information (SI) section 1. Specificity of host/guest interactions is confirmed by quartz crystal microbalance with dissipation monitoring (QCM-D) (SI Figure S2). Each sample is characterized by cyclic voltammetry to quantify Fc density (SI Figure S3), followed by in situ surface plasmon resonance (SPR) characterization to determine adsorbed HA-β-CD

Received: April 6, 2026
Revised: May 7, 2026
Accepted: May 8, 2026
Published: May 19, 2026

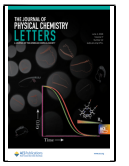

https://doi.org/10.1021/acs.jpclett.6c01096
J. Phys. Chem. Lett. 2026, 17, 6357−6364

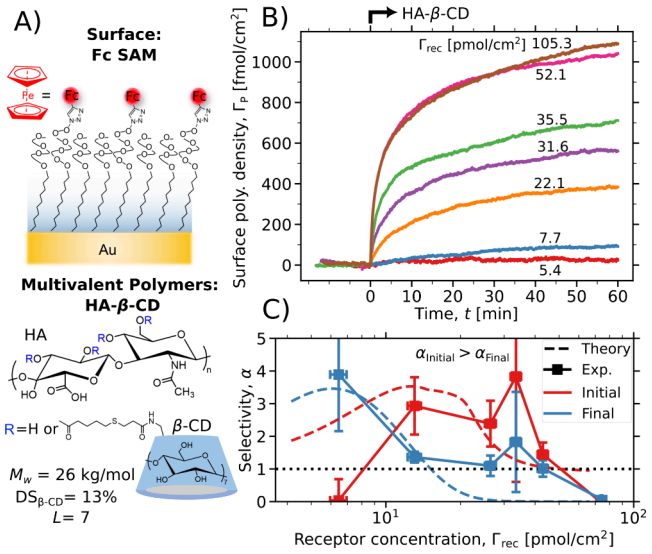

Figure 1. Experimental association kinetics of multivalent polymers. A) The experimental HA-β-CD−Fc SAM system. B,C) Surface polymer density Γ_P determined by SPR and the associated final (blue) and initial (red) selectivity determined by SPR at different Fc surface densities. Electrochemical quantification of Fc density Γ_{rec} and SPR data acquisition and treatment are described in detail in SI section 1. Dashed curves in B,C represent a two-step theory fit of the experimental data, discussed later in the main text.

concentration versus time $\Gamma_P(t)$ (SI Figure S4). The obtained results are summarized in Figure 1B.

To quantify the selectivity of binding under nonequilibrium conditions, we generalize the equilibrium[2,7] definition of selectivity α to depend on observation time t

$$\alpha(t) = \frac{\mathrm{d} \ln \Gamma_P(t)}{\mathrm{d} \ln \Gamma_{rec}} \tag{1}$$

Values of α above unity represent superselectivity, a superlinear dependence of binding on a control parameter, here Γ_{rec}. We calculate the time-dependent selectivity $\alpha(t)$ (SI Figure S5) and define two limiting cases: the initial selectivity $\alpha_{Initial}$ and final selectivity $\alpha_{Final} = \alpha(t_{Final})$ determined at the last data point, which is close to thermodynamic equilibrium and therefore analogous to the Hill coefficient.[2,36] To reduce statistical noise, we define $\alpha_{Initial}$ as the selectivity observed when the surface coverage reaches a predefined fraction (1/4) of the equilibrium (final) value (an alternate definition based on time yields very similar results, see SI Figure S6).

Surprisingly, the experimental system exhibits superselectivity in the initial association ($\alpha_{Initial} > 1$), which significantly exceeds the final, equilibrium selectivity (Figure 1C) for a wide range of receptor densities. The same trend is observed by reanalyzing published experimental data on a similar host/guest system with larger HA-β-CD multivalent probes[35] (SI Figure S9).

To explain these observations, we propose a Langmuir-like model of multivalent kinetics based on previous thermodynamic theory.[2,35] We first investigate one-step binding, where ligand−receptor bond formation occurs in a single reaction step. Multivalent entities (e.g., polymers, nanoparticles) with valency L adsorb from bulk solution onto a receptor covered surface divided into lattice binding sites of volume a^3, for polymers $a^3 = 4\pi R_g^3/3$, with R_g the polymer radius of gyration,[37] and each site contains R_0 surface receptors (Figure 2A). We model multivalent kinetics with a system of ordinary differential equations (ODEs) based on stochastic chemical

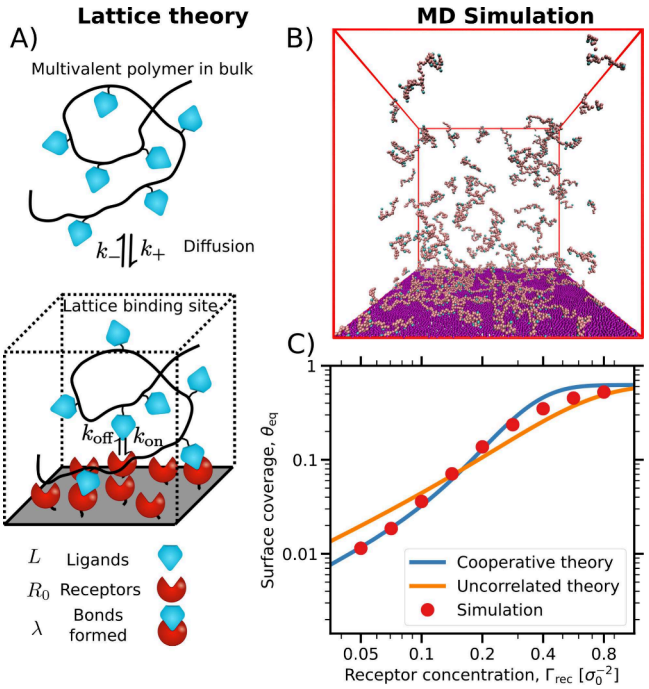

Figure 2. Kinetic theory and MD simulations. (A) Schematic of the developed theory, multivalent polymers adsorb from bulk solution into surface lattice sites with receptors. (B) Example snapshot of MD simulations, multivalent polymers adsorb onto a receptor covered surface. (C) Comparison of equilibrium (final) surface coverage, θ_{eq} between MD simulations (red points) and a one parameter ($\epsilon(1)$) theory fit with uncorrelated binding ($\epsilon(\lambda) = \epsilon(1)$, orange line) and cooperative polymer binding (eq 3, blue line).

kinetics.[38,39] Γ_λ denotes the concentration of surface sites that contain a multivalent entity with λ formed bonds, and its evolution is described by

$$\frac{\mathrm{d}\Gamma_\lambda}{\mathrm{d}t} = k_{off}(\lambda+1)\Gamma_{\lambda+1} - k_{on,\lambda+1}(L-\lambda)(R_0-\lambda)\Gamma_\lambda - k_{off}\lambda\Gamma_\lambda + k_{on,\lambda}(L-\lambda+1)(R_0-\lambda+1)\Gamma_{\lambda-1} \tag{2}$$

The ligand−receptor off rate k_{off} is a constant, while the on rate $k_{on,\lambda}$ can depend on the number of formed bonds due to cooperative binding. For a multivalent entity with no bonds, $\lambda = 0$, the last two terms in eq 2 are replaced with terms for multivalent entity diffusion between surface and bulk solution, $-k_-\Gamma_0 + k_+c_M\Gamma_S$, where $k_+ = Da$ and $k_- = D/a^2$ are the forward and reverse diffusive kinetic constants, with D the diffusion constant of the multivalent entity, Γ_S is the concentration of empty surface binding sites and c_M the bulk multivalent entity concentration (Figure 2A). We solve the system of ODEs to calculate the time evolution of the surface coverage $\theta(t) = \sum_{\lambda=1}^{\min(L,R_0)}\Gamma_\lambda(t)a^2$, and obtain results for a given receptor concentration Γ_{rec}, via a (Poisson) distribution of R_0. Surface coverage is proportional to the polymer molar density obtained from experiment, $\theta(t) = \Gamma_P(t)N_Aa^2$, with N_A being Avogadro's constant. Additional details can be found in SI section 2.

Previous thermodynamic models of multivalent binding have mostly considered the free energy of bond formation to be a constant. Multivalent nanoparticle binding can be described

https://doi.org/10.1021/acs.jpclett.6c01096
J. Phys. Chem. Lett. 2026, 17, 6357−6364

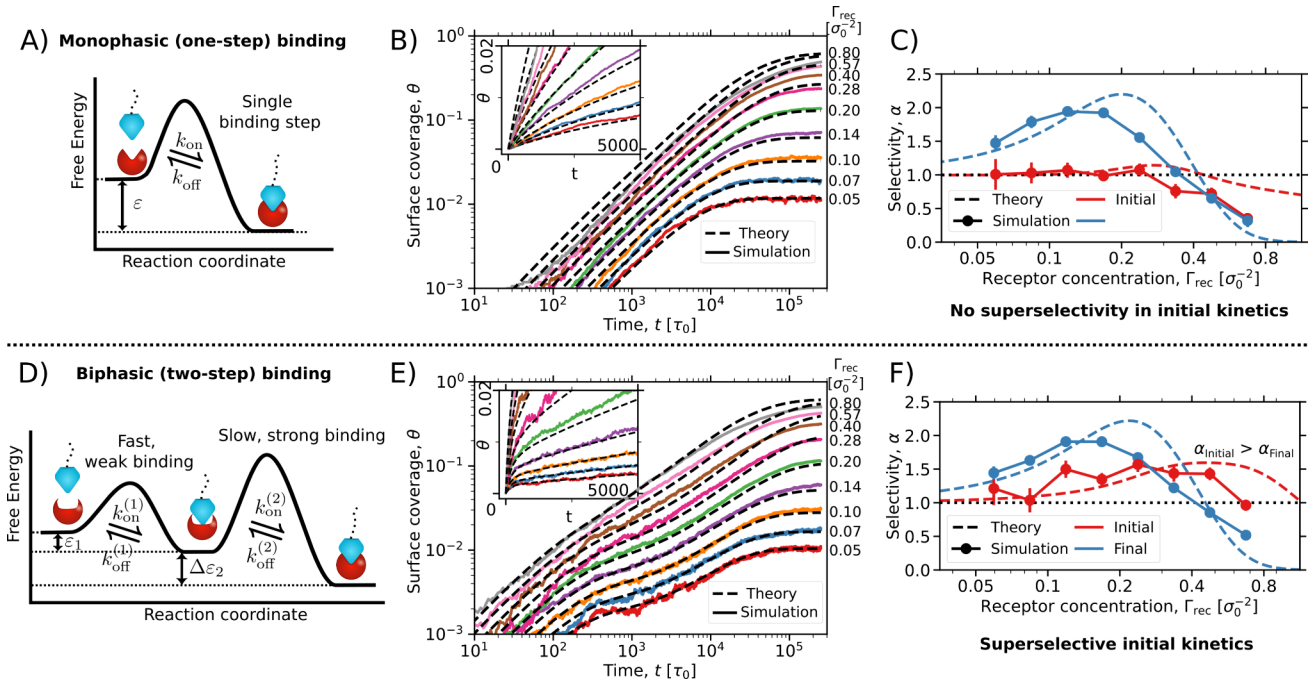

Figure 3. Modeling multivalent kinetics. (A) Reaction barrier schematic for one-step (monophasic) binding. (B,C) Surface coverage and associated selectivity obtained from one-step MD simulations (full lines with markers) and theoretical model (dashed lines). (D) Two-step (biphasic) binding features formation of an intermediate complex followed by a slower reaction to a more stable complex. (E,F) Surface coverage and the associated selectivity for two-step MD simulations. Insets in (B,E) show a zoom in at small surface coverages on a linear plot. Dotted black lines in (C,F) represent selectivity $\alpha = 1$, above which lies the superselective regime. Theory fitted to one-step MD data ($\theta(t)$) with two fitting parameters ($\epsilon(1)$, k_{on}), and to two-step MD data with four parameters, ($\epsilon(1)$, $k_{on}^{(1)}$, $\Delta\epsilon_2$, $k_{on}^{(2)}$).

relatively well by this assumption,[2,40] however, multivalent polymers exhibit cooperative effects. Ligand binding brings the polymer backbone closer to the surface, which facilitates further ligand binding and increases selectivity.[35,41] To calculate these effects we derive a scaling theory for cooperative polymer binding. The volume that unbound ligands can explore depends on the average loop size of the bound polymer backbone, and the on-rate is inversely proportional to this free ligand volume. The radius of gyration of the average loop is $R_{g,loop}(\lambda) \sim R_g/\lambda^{\nu}$ and the free volume that unbound ligands can explore is $\sim(R_{g,loop})^3$. Therefore, we obtain the on rate for λ-th bond formation $k_{on,\lambda} = k_{on}\lambda^{3\nu}$, with k_{on} the on rate for first bond formation and ν the polymer scaling exponent. Here we use $\nu = 0.5$ because the polymer is semiflexible. The free energy of λ-th bond formation $\epsilon(\lambda)$ is determined by the ratio of the rates: $\beta\epsilon(\lambda) = -\ln(k_{on,\lambda}/k_{off})$, with $\beta = 1/k_BT$, k_B the Boltzmann constant and T the absolute temperature. The bond strength thus increases the more bonds are formed

$$\beta\epsilon(\lambda) = \beta\epsilon(1) - 3\nu \ln(\lambda) \tag{3}$$

with $\epsilon(1)$ the free energy to form the first bond for an unbound polymer at the surface.

The model is validated with MD simulations of bead−spring polymers adsorbing to a surface with the polymer bead diameter, $\sigma_0 = 1$ nm, and 48 beads per polymer to match the experimental contour length (Figure 2B, see methods, SI section 3 for details). The derived cooperative theory explains equilibrium MD results very well, significantly better than a description with uncorrelated binding ($\epsilon(\lambda) = \epsilon(1)$), which ignores polymer cooperative effects (Figure 2C).

Cooperative theory and MD simulations also show very good agreement in adsorption kinetics (Figure 3), with deviations occurring only at very high receptor density ($\Gamma_{rec} \gtrsim \sigma_0^{-2}$) where receptor crowding reduces the association rate (Figure 3B). Additionally, eq 3 slightly overestimates polymer cooperativity (see SI, section 4.1), leading to overestimation at strong binding. While this system exhibits superselectivity in equilibrium, the initial, kinetic selectivity in association dynamics is not superselective, $\alpha_{Initial} \lesssim 1$ (Figure 3C). This result can be intuitively understood because the association rate is determined by the formation of the first bond between the multivalent entity and surface receptors, the rate of which is proportional to the receptor concentration, so we expect $\alpha_{Initial} \approx 1$ for a reaction-limited case (and $\alpha_{Initial} \approx 0$ for the diffusion-limited case where association is independent of surface properties). This is supported by the fact that multivalent avidity effects arise primarily due to decreased unbinding rates,[14,26,27] while the total reaction forward rate increases only linearly with the number of ligands[25] (see SI section 4). However, $\alpha_{Initial} \approx 1$ is inconsistent with our experimental data (Figure 1C) which clearly show a superselective kinetic response.

As one-step multivalency fails to exhibit superselectivity in association kinetics, we investigate biphasic, two-step binding, commonly observed in various kinetics studies.[42] The main feature of two-step binding is an initial, rapid formation of an intermediate complex, followed by slower formation of a more stable complex. Such binding is found in many supramolecular and biological systems, where the formation of the stable complex is usually accompanied by a slow conformational change in the receptor (induced-fit model).[43] We extend the theoretical model to include two-step ligand−receptor binding

https://doi.org/10.1021/acs.jpclett.6c01096
J. Phys. Chem. Lett. 2026, 17, 6357−6364

(Figure 3D). The microscopic on and off reaction rates between unbound ligands and receptors and the intermediate bound state are $k_{on,\lambda}^{(1)}$, $k_{off}^{(1)}$, while reaction rates between the intermediate and the stable state are denoted by $k_{on}^{(2)}$, $k_{off}^{(2)}$. The free energy of intermediate bond formation is $\epsilon_1(\lambda)$, while the free energy change for forming the stable bond from the intermediate state is $\Delta\epsilon_2$, where $k_{on,\lambda}^{(1)}/k_{off}^{(1)} = \exp(-\beta\epsilon_1(\lambda))$ and $k_{on}^{(2)}/k_{off}^{(2)} = \exp(-\beta\Delta\epsilon_2)$. Cooperative effects depend on the total number of formed bonds, $\lambda = i + j$, analogously to the one-step model, see methods eq 5.

We validate the two-step model via MD simulations, performing an identical set of MD simulations as before, changing only the ligand−receptor interaction potential to feature an additional higher barrier within the potential. Theory and MD show excellent agreement, see Figures 3E,F. Comparing the two-step and one-step cases, the equilibrium results are nearly identical, as thermodynamically, the two-step model is exactly equal to the monophasic model with a rescaled free energy of bond formation, $\beta\epsilon(\lambda) = -\ln[\exp(-\beta\epsilon_1(\lambda)) + \exp(-\beta(\epsilon_1(\lambda) + \Delta\epsilon_2))]$. However, the kinetic response of two-step binding is superselective ($\alpha_{Initial} > 1$), and we observe a range where the initial selectivity is significantly higher than the equilibrium selectivity (Figure 3F). This kinetic superselectivity is achieved on a range of time scales t that fall between the formation of the weak intermediate bond and equilibration, $1/(k_{on}^{(1)} L R_0 c_M a^3) \lesssim t \lesssim 1/k_{on}^{(2)}$.

The kinetic superselectivity arises because the system initially reaches a multivalent pseudoequilibrium dictated solely by the intermediate, fast interactions, before the binding slowly proceeds to the true equilibrium dictated by the slower, stable interactions. This pseudoequilibrium features a selectivity maximum at a higher receptor concentration compared to the full equilibrium (Figures 1C,F). As a result, there exists a range of receptor concentrations where the pseudoequilibrium selectivity is larger than the equilibrium selectivity. Viewing the binding process through the rate-determining step (RDS), if the RDS occurs in the initial stages of the binding (diffusion, first bond formation) we cannot expect kinetic superselectivity, contrary to if the RDS occurs when binding is already multivalent. This phenomenon is not limited to a two-step binding model, and we expect a qualitatively similar effect for any combination of multivalent weak, fast and slow, strong interactions (see SI Figure S15). Intriguingly, even if the equilibrium binding is very strong (e.g., covalent), the system would still exhibit kinetic superselectivity. Thereby, superselective binding should not be limited to weak bonds as previously thought.[2,7,28]

While the two-step binding model of fast and slow interactions can explain the observed kinetic superselectivity (Figure 1C), the exact chemical mechanism responsible for these observations remains an open question. We speculate the two-step binding behavior originates from a weak, hydrophobic interaction between the modified polymer and Fc, while β-CD−Fc host−guest binding represents the strong binding step. The weak, nonspecific interactions may be mediated by the primarily hydrophobic linker between β-CD and HA (see Figure 1A). This is supported by observation of weak adsorption of HA-β-CD to a hydrophobic surface composed of purely alkyl SAM (SI Figure S3C,D), suggesting similar interaction is present on the hydrophobic Fc SAM.

In addition to SPR experiments, which are limited by the maximum injection volume, we performed a set of QCM-D in situ coupled with spectroscopic ellipsometry (SE) experiments (Figures S7,S8) employing the same Fc SAM, HA-β-CD system to study longer dissociation kinetics (Figure 4A).

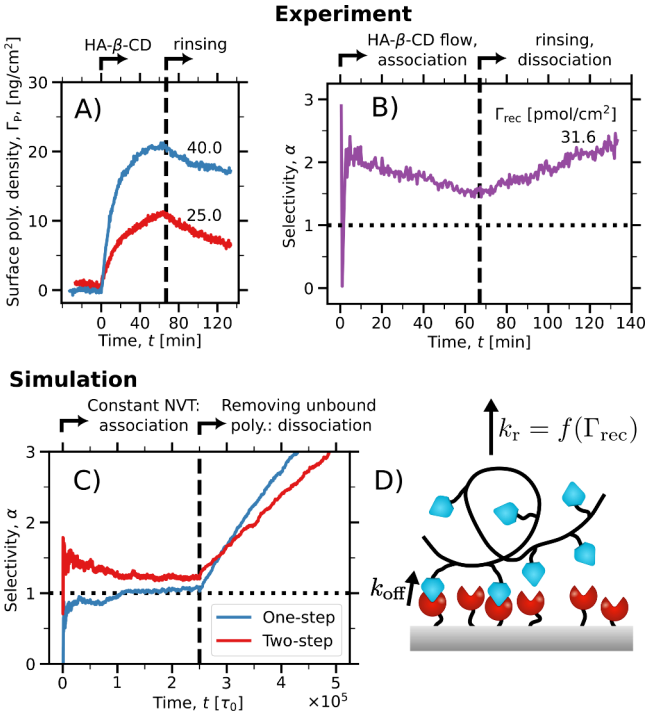

Figure 4. Selectivity in association and dissociation. (A,B) Surface density and the associated selectivity time dependence measured by QCM-D−SE. At t = 67 min the polymer solution is replaced by its aqueous medium and dissociation begins. (C) MD simulations selectivity time dependence for one-step (blue) and two-step (red) ligand−receptor binding. (D) The total dissociation rate constant, k_r, decreases with receptor concentration, resulting in increasing dissociation selectivity.

Interestingly, the dissociation process is also more selective than the equilibrium interaction in both experiments and MD simulations (Figures 4B,C). We explain this phenomenon by approximating the dissociation binding curve as a first order exponential function $\theta(t) = \theta_{eq}\exp(-k_r t)$, where θ_{eq} is the surface density at the beginning of the dissociation and k_r the effective unbinding rate constant for the multivalent entities. Because the binding is multivalent, k_r decreases with receptor density (Figure 4D). This results in a linear increase in dissociation selectivity with time, $\alpha(t) = \alpha_{eq} - \frac{dk_r}{d\ln\Gamma_{rec}} t$, where $\frac{dk_r}{d\ln\Gamma_{rec}} < 0$, in agreement with both experiment and MD simulation data. The selectivity will thus be maximized when the surface is completely empty, $\theta \to 0$, which is likely not very useful. However, if we ask what is the maximal selectivity at a given value of θ, it turns out the largest selectivity is achieved in a dissociation process. In the strong binding limit the surface is initially fully covered, $\theta_{eq} \to 1$, and we can derive $k_r \propto \Gamma_{rec}^{-L}$ (SI section 2.5). Thereby, the maximal dissociation selectivity at a given θ is

$$\alpha^{max}(\theta) = -L \ln[\theta(t)] \quad (4)$$

Whereas the equilibrium and association selectivity are limited by valency,[2,36] $\alpha_{eq} \leq L$, the selectivity in dissociation can surpass L for $\theta(t) < 0.3$.

https://doi.org/10.1021/acs.jpclett.6c01096
J. Phys. Chem. Lett. 2026, 17, 6357−6364

The multivalent equilibrium selective response depends on the master, scaling variable,[2,35] and our kinetic model also predicts identical behavior for different systems with an identical value of a scaling variable, $\gamma = R_0 k_{on}/k_{off}$, provided that the off rate, k_{off}, is kept constant (and assuming an abundance of receptors, $R_0 \gg L$, see SI section 2.3). Thus, while the experimental and simulation results demonstrate kinetic selectivity to receptor concentration, we expect the results to be general across other control parameters such as bond strength, valency, temperature, or presence of cofactors or competitors.[7,44]

We demonstrate the behavior of selectivity at a given value of surface coverage, θ_c, by comparing $\alpha(\theta_c)$ as a function of the multivalent scaling variable γ in association and dissociation kinetics, as well as when θ_c is the equilibrium surface coverage (Figure 5). As expected from the previous discussion, the highest selectivity at a given surface density θ_c is obtained in dissociation kinetics. Association and dissociation show opposite behavior for both one-step, two-step, and diffusion limited cases; when one is high, the other is low. We can understand the reversed effects by considering that the equilibrium value is obtained by the ratio of the association and dissociation rates, therefore, if selectivity in one increases it must decrease in the other, resulting in the mirroring between association/dissociation results around the equilibrium value. Interestingly, the dissociation selectivity is higher when binding is diffusion-limited, compared to reaction-limited. Under diffusion limited conditions, polymers can rebind at the surface and the probability of rebinding depends on the scaling variable, thus increasing the dissociation selectivity (see SI section 2.5). Notably, in the two-step binding case, the association selectivity can exceed the equilibrium selectivity, however, this results in a corresponding decrease in dissociation selectivity. We expect similar behavior for other models exhibiting association kinetic supreselectivity, e.g. when ligands have two distinct binding modes.

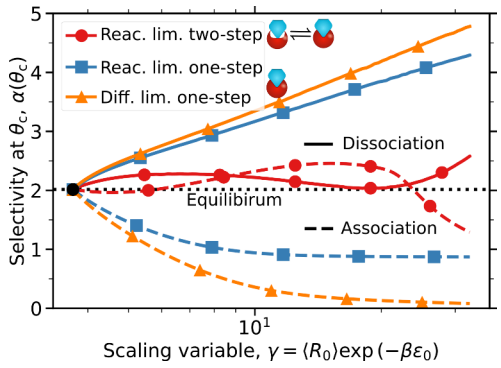

Figure 5. Selectivity at a given value of surface coverage, θ_c. Black dotted line shows equilibrium selectivity. Full, dashed lines show selectivity in dissociation, association kinetics, respectively. Blue squares represent reaction-limited ($D \to \infty$) monophasic binding, orange triangles show diffusion-limited monophasic binding ($D = 10^3 \sigma_0^2 \tau_0^{-1}$), and red circles shows reaction-limited two-step binding. Parameters: $\theta_c = 0.25$, $L = 5$, $R_g = 5\sigma_0$, $c_M = 10^{-6}\sigma_0^{-3}$, uncorrelated binding, $\beta\epsilon(\lambda) = 0$, $k_{on,\lambda} = 1\ \tau_0^{-1}$. Two-step binding parameters: $\beta\Delta\epsilon_2 = -2$, $k_{on}^{(2)}/k_{on,1}^{(1)} = 0.01$.

In conclusion, we identified pronounced superselectivity in association kinetics of multivalent polymers, which we explain using a two-step binding model that features a combination of fast, weak and slow, strong interactions. This finding introduces a new approach: superselective targeting based on the association rate rather than the equilibrium state, which should be very useful in systems where equilibrium is difficult to achieve. Moreover, this finding can be applied to introduce (kinetic) superselectivity to systems where equilibrium superselectivity is impossible, such as very strong (covalent) interactions. We find that high kinetic selectivity in association is achieved on a time scale t that falls between the formation of the weak and strong bonds, for two-step binding $1/(k_{on}^{(1)} L R_0 c_M a^3) \lesssim t \lesssim 1/k_{on}^{(2)}$. Therefore, a large window of high kinetic selectivity is obtained when the rate of weak bond formation $k_{on}^{(1)}$ is much faster than the rate of strong binding $k_{on}^{(2)}$.

We demonstrated that selectivity in a dissociation process increases linearly with time, and surpasses the equilibrium selectivity. This leads to a surprising result that the maximal possible selectivity is achieved by fully saturating the surface and waiting for dissociation. In analogy with equilibrium predictions, we show that the kinetic selectivity is a general feature of multivalent interactions and extends to other control parameters beside receptor concentration.

Practically, in the body, cells can endocytose macromolecular or nanoparticle based drugs on a time scale of seconds to minutes. If endocytosis time is comparable or faster than drug binding, then equilibrium is never achieved and therefore targeting selectivity is determined by the association rate selectivity, rather than equilibrium selectivity. On the other hand, many cellular processes require that a ligand is bound for a sufficient amount of time to trigger a response. In this case, targeting cells based on dissociation rate may yield optimal selectivity. More broadly, our results provide fundamental understanding of multivalent kinetics. The kinetic theory presented here should be useful to engineer selective multivalent interactions in biological or synthetic systems that operate out of equilibrium.

METHODS

Self-assembled monolayer formation and functionalization with ferrocene through the azide−alkyne click reaction was accomplished using previously developed protocols.[34,45] HA-β-CD was synthesized by thiolene coupling between HA-pentenoate and β-CD-thiol.[34,37] The HA-β-CD average molecular weight, the average distance between β-CDs along the contour of the polymer chain, and the average number of β-CDs per polymer chain were calculated to be M_w = 26 kg/mol, $d_{\beta-CD}$ = 7 nm, and L = 7 (degree of substitution, $DS_{\beta-CD}$ = 0.13). Cyclic voltammetry was used to quantify Fc surface density in the formed SAM-Fc. Electrochemical measurements were carried out following previously established procedures using a three-electrode potentiostatic system.[45] The areal density of Fc was modulated (Γ_{rec}), and the binding response was studied via surface plasmon resonance (SPR) upon the injection of a fixed concentration c_M = 50 μg/mL of HA-β-CD. Over extended time intervals, quartz crystal microbalance with dissipation monitoring (QCM-D) enabled real-time monitoring of HA-β-CD binding and its subsequent desorption during rinsing. Spectroscopic ellipsometry was in situ coupled with QCM-D to monitor the adsorption of HA-β-CD and to establish a calibration curve correlating QCM-D frequency shifts with the corresponding adsorbed dry mass.[46] Additional details are available in the Supporting Information section 1.

The developed theoretical model of multivalent binding kinetics is described in the main text eq 2, the derived expression for polymer cooperativity is given by eq 3. The extended two-step model (Figure 3D) tracks the concentration of states with i intermediate bonds, and j stable bonds, $\Gamma_{i,j}$

https://doi.org/10.1021/acs.jpclett.6c01096
J. Phys. Chem. Lett. 2026, 17, 6357−6364

$$\frac{d\Gamma_{i,j}}{dt} = (i+1)k_{off}^{(1)}\Gamma_{i+1,j} - k_{on,\lambda+1}^{(1)}(L-\lambda)(R_0-\lambda)\Gamma_{i,j} - ik_{off}^{(1)}\Gamma_{i,j} + k_{on,\lambda}^{(1)}(L-\lambda+1)(R_0-\lambda+1)\Gamma_{i-1,j} + (j+1)k_{off}^{(2)}\Gamma_{i-1,j+1} - ik_{on}^{(2)}\Gamma_{i,j} - jk_{off}^{(2)}\Gamma_{i,j} + (i+1)k_{on}^{(2)}\Gamma_{i+1,j-1} \quad (5)$$

with $\lambda = i + j$. $\Gamma_{0,0}$ includes the diffusive contribution ($-k\_\Gamma_{0,0} + k_+c_M\Gamma_S$), while terms not originating from or leading toward valid states ($i + j \leq \min(L,R_0)$, $i,j \geq 0$) are omitted. We include cooperative effects in the formation of the intermediate bonds, $k_{on,\lambda}^{(1)} = k_{on,1}^{(1)}\lambda^{3\nu}$, based on the total number of formed bonds, $\lambda = i + j$. The Supporting Information section 2 contains additional detail about the kinetic and associated thermodynamic equilibrium model, derivation of scaling variable, and additional comparison between model and experimental results. Theory fit parameters to experimental data in Figure 1C are $\beta\epsilon(1) = 3.96$, $\beta\Delta\epsilon_2 = -0.56$, $k_{on,1}^{(1)} = 2.20 \times 10^{-3}$ s^{-1}, $k_{on}^{(2)} = 2.72 \times 10^{-4}$ s^{-1}. In Figure 3B,C to one-step MD data the fit parameters are given by $\beta\epsilon(1) = 4.79$, $k_{on,1} = 1.71 \times 10^{-6}\tau_0^{-1}$, and in Figure 3E,F the fit parameters to two-step MD data are $\beta\epsilon(1) = 4.88$, $\beta\Delta\epsilon_2 = -1.30$, $k_{on,1}^{(1)} = 7.92 \times 10^{-6}\tau_0^{-1}$, $k_{on}^{(2)} = 2.72 \times 10^{-4}\tau_0^{-1}$.

We employ LAMMPS[47] to perform constant *NVT* molecular dynamics (MD) simulations of a bead−spring multivalent polymer binding to a receptor-decorated surface. We use the polymer bead diameter, σ_0, (σ_0 = 1 nm) as the length unit scale of the simulations, while τ_0 is the time unit (τ_0 = 0.44 ns). We simulate a cubic box 100 σ_0 to a side with 100 flexible polymers consisting of 48 backbone beads and L = 8 ligand beads randomly distributed along the backbone. The polymer concentration is $c_M = 10^{-4}\sigma_0^{-3}$. We apply periodic boundary conditions in two spatial directions, while the third contains repulsive walls, one of which carries point like receptors which can interact with ligand beads on polymers. Ligand−receptor binding is described by a spherically symmetric potential which features an additional potential barrier in the case of two-step binding (cf. Figures 3A,D, see SI Figure S21). Receptors are stationary, not integrated during the production simulations, and are equilibrated via two-dimensional simulations with receptor size $\sigma_{rec} = \sigma_0$ with WCA potential to prevent ligand binding to multiple receptors or vice versa. Before the association production runs, polymers were randomly distributed in the simulation box and equilibrated without the presence of receptors. Dissociation production runs began from the end points of association runs. We simulate a dissociative (zero bulk concentration) environment by periodically deleting any polymers above a height threshold from the simulation. During production simulations, we track the number of formed ligand−receptor bonds, as well as the number of bound polymers. We average our results over a number of parallel simulations to reduce statistical noise. Full details are provided in the Supporting Information section 3. To speed up MD simulations and enable exploration of relevant time scales, we use 100-fold larger polymer bulk concentration in the simulations compared to experiments. As a consequence, the selectivity in the experimental data is higher compared to the MD data (compare Figures 1C and 3F), as higher concentration reduces selectivity.[7]

■ ASSOCIATED CONTENT

Supporting Information

The Supporting Information is available free of charge at https://pubs.acs.org/doi/10.1021/acs.jpclett.6c01096.

- Additional details about the experiments, the theoretical model of multivalent binding kinetics, molecular dynamics simulations, and further comparisons between simulation and theory results (PDF)

■ AUTHOR INFORMATION

Corresponding Authors

Galina V. Dubacheva − *Département de Chimie Moléculaire, Université Grenoble Alpes, 38000 Grenoble, France;* orcid.org/0000-0003-1417-5381; Email: galina.dubacheva@univ-grenoble-alpes.fr

Tine Curk − *Department of Materials Science and Engineering, Johns Hopkins University, Baltimore, Maryland 21218, United States; Department of Physics and Astronomy and Institute for NanoBioTechnology, Johns Hopkins University, Baltimore, Maryland 21218, United States;* orcid.org/0000-0002-2167-5336; Email: tcurk@jhu.edu

Authors

Vid Ravnik − *Faculty of Chemistry and Chemical Engineering, University of Maribor, 2000 Maribor, Slovenia;* orcid.org/0000-0001-5605-3345

Baptiste Chabaud − *Département de Chimie Moléculaire, Université Grenoble Alpes, 38000 Grenoble, France*

Urban Bren − *Faculty of Chemistry and Chemical Engineering, University of Maribor, 2000 Maribor, Slovenia; The Faculty of Mathematics, Natural Sciences and Information Technologies, University of Primorska, 6000 Koper, Slovenia; Institute for Environmental Protection and Sensors, 2000 Maribor, Slovenia;* orcid.org/0000-0002-8806-3019

Complete contact information is available at: https://pubs.acs.org/10.1021/acs.jpclett.6c01096

Notes

The authors declare no competing financial interest.

■ ACKNOWLEDGMENTS

V.R. and U.B. gratefully acknowledge financial support from the Slovenian Research and Innovation Agency (ARIS) through project and program grants P1-0403, P2-0438, J1-4398, and L7-60161. U.B. also acknowledges the Fulbright foundation for funding his research visit at Johns Hopkins University. G.V,D. and B.C. acknowledge ANR JCJC "Supra-Switch" funding (ANR-18-CE09-0009) and ICMG FR2607 Chemistry Nanobio Platform (UGA, Grenoble). Angline van Der Heyden (DCM, UGA, Grenoble) is acknowledged for her help with SPR experiments. T.C. acknowledges support from the National Science Foundation, CBET Division, Biosensors Program, Award Number 2402407. Computational work was carried out at HPC Vega and the Advanced Research Computing at Hopkins (ARCH) core facility (rockfish.jhu.edu), which is supported by the National Science Foundation (NSF) grant number OAC 1920103.

■ REFERENCES

(1) Mammen, M.; Choi, S.-K.; Whitesides, G. M. Polyvalent interactions in biological systems: implications for design and use of multivalent ligands and inhibitors. *Angew. Chem., Int. Ed.* **1998**, *37*, 2754−2794.

(2) Martinez-Veracoechea, F. J.; Frenkel, D. Designing super selectivity in multivalent nano-particle binding. *Proc. Natl. Acad. Sci. U. S. A.* **2011**, *108*, 10963−10968.

(3) Carlson, C. B.; Mowery, P.; Owen, R. M.; Dykhuizen, E. C.; Kiessling, L. L. Selective tumor cell targeting using low-affinity, multivalent interactions. *ACS Chem. Biol.* **2007**, *2*, 119−27.

(4) Wang, J.; Min, J.; Eghtesadi, S. A.; Kane, R. S.; Chilkoti, A. Quantitative Study of the Interaction of Multivalent Ligand-Modified

Nanoparticles with Breast Cancer Cells with Tunable Receptor Density. *ACS Nano* **2020**, *14*, 372−383.
(5) Tian, X.; Angioletti-Uberti, S.; Battaglia, G. On the design of precision nanomedicines. *Science advances* **2020**, *6*, eaat0919.
(6) Woythe, L.; Tito, N. B.; Albertazzi, L. A quantitative view on multivalent nanomedicine targeting. *Advanced drug delivery reviews* **2021**, *169*, 1−21.
(7) Dubacheva, G. V.; Curk, T.; Richter, R. P. Determinants of superselectivity - practical concepts for application in biology and medicine. *Accounts of chemical research* **2023**, *56*, 729−739.
(8) Kitov, P. I.; Bundle, D. R. On the nature of the multivalency effect: a thermodynamic model. *J. Am. Chem. Soc.* **2003**, *125*, 16271−16284.
(9) Diestler, D.; Knapp, E. Statistical thermodynamics of the stability of multivalent ligand-receptor complexes. *Physical review letters* **2008**, *100*, 178101.
(10) Csizmar, C. M.; Petersburg, J. R.; Perry, T. J.; Rozumalski, L.; Hackel, B. J.; Wagner, C. R. Multivalent ligand binding to cell membrane antigens: defining the interplay of affinity, valency, and expression density. *J. Am. Chem. Soc.* **2019**, *141*, 251−261.
(11) Li, S.; Lou, Y.; Bastings, M. M. Multivalent engineering of bio interfaces with DNA-based nanomaterials. *Adv. Drug Delivery Rev.* **2025**, *225*, 115681.
(12) Mulder, A.; Huskens, J.; Reinhoudt, D. N. Multivalency in supramolecular chemistry and nanofabrication. *Organic & biomolecular chemistry* **2004**, *2*, 3409−3424.
(13) Long, M.; Lü, S.; Sun, G. Kinetics of receptor-ligand interactions in immune responses. *Cell Mol. Immunol* **2006**, *3*, 79−86.
(14) Munoz, E. M.; Correa, J.; Riguera, R.; Fernandez-Megia, E. Real-time evaluation of binding mechanisms in multivalent interactions: a surface plasmon resonance kinetic approach. *J. Am. Chem. Soc.* **2013**, *135*, 5966−5969.
(15) An, C.; Wang, X.; Song, F.; Hu, J.; Li, L. Insights into intercellular receptor-ligand binding kinetics in cell communication. *Frontiers in Bioengineering and Biotechnology* **2022**, *10*, 953353.
(16) Huang, J.; Zarnitsyna, V. I.; Liu, B.; Edwards, L. J.; Jiang, N.; Evavold, B. D.; Zhu, C. The kinetics of two-dimensional TCR and pMHC interactions determine T-cell responsiveness. *Nature* **2010**, *464*, 932−936.
(17) Liu, B.; Chen, W.; Evavold, B. D.; Zhu, C. Accumulation of dynamic catch bonds between TCR and agonist peptide-MHC triggers T cell signaling. *Cell* **2014**, *157*, 357−368.
(18) Wu, P.; Zhang, T.; Liu, B.; Fei, P.; Cui, L.; Qin, R.; Zhu, H.; Yao, D.; Martinez, R. J.; Hu, W.; et al. Mechano-regulation of peptide-MHC class I conformations determines TCR antigen recognition. *Molecular cell* **2019**, *73*, 1015−1027.
(19) Stylianopoulos, T.; Jain, R. K. Design considerations for nanotherapeutics in oncology. *Nanomedicine: Nanotechnology, Biology and Medicine* **2015**, *11*, 1893−1907.
(20) Foster, C.; Watson, A.; Kaplinsky, J.; Kamaly, N. Improved targeting of cancers with nanotherapeutics. *Cancer Nanotechnology: Methods and Protocols* **2017**, *1530*, 13−37.
(21) Shao, X.; Shi, C.; Wu, S.; Wang, F.; Li, W. Review of the pharmacokinetics of nanodrugs. *Nanotechnol. Rev.* **2023**, *12*, 20220525.
(22) McCann, B.; Tipper, B.; Shahbeigi, S.; Soleimani, M.; Jabbari, M.; Nasr Esfahani, M. A Review on Perception of Binding Kinetics in Affinity Biosensors: Challenges and Opportunities. *ACS omega* **2025**, *10*, 4197−4216.
(23) Lanfranco, R.; Jana, P. K.; Tunesi, L.; Cicuta, P.; Mognetti, B. M.; Di Michele, L.; Bruylants, G. Kinetics of nanoparticle-membrane adhesion mediated by multivalent interactions. *Langmuir* **2019**, *35*, 2002−2012.
(24) Schulte, C.; Soldà, A.; Spänig, S.; Adams, N.; Bekić, I.; Streicher, W.; Heider, D.; Strasser, R.; Maric, H. M. Multivalent binding kinetics resolved by fluorescence proximity sensing. *Communications biology* **2022**, *5*, 1070.
(25) Hong, S.; Leroueil, P. R.; Majoros, I. J.; Orr, B. G.; Baker, J. R.; Holl, M. M. B. The binding avidity of a nanoparticle-based multivalent targeted drug delivery platform. *Chemistry & biology* **2007**, *14*, 107−115.
(26) Tassa, C.; Duffner, J. L.; Lewis, T. A.; Weissleder, R.; Schreiber, S. L.; Koehler, A. N.; Shaw, S. Y. Binding affinity and kinetic analysis of targeted small molecule-modified nanoparticles. *Bioconjugate Chem.* **2010**, *21*, 14−19.
(27) Choi, S. K.; Myc, A.; Silpe, J. E.; Sumit, M.; Wong, P. T.; McCarthy, K.; Desai, A. M.; Thomas, T. P.; Kotlyar, A.; Holl, M. M. B.; et al. Dendrimer-based multivalent vancomycin nanoplatform for targeting the drug-resistant bacterial surface. *ACS Nano* **2013**, *7*, 214−228.
(28) Scheepers, M.; van IJzendoorn, L.; Prins, M. Multivalent weak interactions enhance selectivity of interparticle binding. *Proc. Natl. Acad. Sci. U. S. A.* **2020**, *117*, 22690−22697.
(29) Hoogerheide, D. P.; Bezrukov, S. M. Logarithmic Binding and Stretched-Exponential Kinetics in Peripheral Protein Interactions with Lipid Membrane Surfaces. *J. Phys. Chem. Lett.* **2026**, *17*, 3917.
(30) Müller, K. M.; Arndt, K. M.; Plückthun, A. Model and simulation of multivalent binding to fixed ligands. *Analytical biochemistry* **1998**, *261*, 149−158.
(31) Vauquelin, G.; Charlton, S. J. Exploring avidity: understanding the potential gains in functional affinity and target residence time of bivalent and heterobivalent ligands. *British journal of pharmacology* **2013**, *168*, 1771−1785.
(32) Errington, W. J.; Bruncsics, B.; Sarkar, C. A. Mechanisms of noncanonical binding dynamics in multivalent protein-protein interactions. *Proc. Natl. Acad. Sci. U. S. A.* **2019**, *116*, 25659−25667.
(33) Bruncsics, B.; Errington, W. J.; Sarkar, C. A. MVsim is a toolset for quantifying and designing multivalent interactions. *Nat. Commun.* **2022**, *13*, 5029.
(34) Chabaud, B.; Bonnet, H.; Lartia, R.; Van Der Heyden, A.; Auzély-Velty, R.; Boturyn, D.; Coche-Guérente, L.; Dubacheva, G. V. Influence of Surface Chemistry on Host/Guest Interactions: A Model Study on Redox-Sensitive β-Cyclodextrin/Ferrocene Complexes. *Langmuir* **2024**, *40*, 4646−4660.
(35) Dubacheva, G. V.; Curk, T.; Auzély-Velty, R.; Frenkel, D.; Richter, R. P. Designing multivalent probes for tunable superselective targeting. *Proc. Natl. Acad. Sci. U. S. A.* **2015**, *112*, 5579−5584.
(36) Curk, T.; Dobnikar, J.; Frenkel, D. *Multivalency: Concepts, Research & Applications*; John Wiley & Sons, Ltd: 2018; Chapter 3, pp 75−101.
(37) Dubacheva, G. V.; Curk, T.; Mognetti, B. M.; Auzély-Velty, R.; Frenkel, D.; Richter, R. P. Superselective targeting using multivalent polymers. *J. Am. Chem. Soc.* **2014**, *136*, 1722−1725.
(38) McQuarrie, D. A. Stochastic approach to chemical kinetics. *Journal of applied probability* **1967**, *4*, 413−478.
(39) Gillespie, D. T. Stochastic simulation of chemical kinetics. *Annu. Rev. Phys. Chem.* **2007**, *58*, 35−55.
(40) Curk, T.; Dobnikar, J.; Frenkel, D. Optimal multivalent targeting of membranes with many distinct receptors. *Proc. Natl. Acad. Sci. U. S. A.* **2017**, *114*, 7210−7215.
(41) Ravnik, V.; Bren, U.; Curk, T. Designing Multivalent Copolymers for Selective Targeting of Multicomponent Surfaces. *Macromolecules* **2024**, *57*, 5991−6002.
(42) Tiwari, P. B.; Wang, X.; He, J.; Darici, Y. Analyzing surface plasmon resonance data: choosing a correct biphasic model for interpretation. *Rev. Sci. Instrum.* **2015**, *86*, 035001.
(43) Koshland, D. E., Jr The key-lock theory and the induced fit theory. *Angewandte Chemie International Edition in English* **1995**, *33*, 2375−2378.
(44) Curk, T.; Dubacheva, G. V.; Brisson, A. R.; Richter, R. P. Controlling superselectivity of multivalent interactions with cofactors and competitors. *J. Am. Chem. Soc.* **2022**, *144*, 17346−17350.
(45) Dubacheva, G. V.; Van Der Heyden, A.; Dumy, P.; Kaftan, O.; Auzély-Velty, R.; Coche-Guerente, L.; Labbé, P. Electrochemically controlled adsorption of Fc-functionalized polymers on β-CD-modified self-assembled monolayers. *Langmuir* **2010**, *26*, 13976−13986.

https://doi.org/10.1021/acs.jpclett.6c01096
J. Phys. Chem. Lett. 2026, 17, 6357−6364

(46) Kirichuk, O.; Srimasorn, S.; Zhang, X.; Roberts, A. R.; Coche-Guerente, L.; Kwok, J. C.; Bureau, L.; Débarre, D.; Richter, R. P. Competitive specific anchorage of molecules onto surfaces: quantitative control of grafting densities and contamination by free anchors. *Langmuir* **2023**, *39*, 18410−18423.
(47) Thompson, A. P.; Aktulga, H. M.; Berger, R.; Bolintineanu, D. S.; Brown, W. M.; Crozier, P. S.; in 't Veld, P. J.; Kohlmeyer, A.; Moore, S. G.; Nguyen, T. D.; Shan, R.; Stevens, M. J.; Tranchida, J.; Trott, C.; Plimpton, S. J. LAMMPS - a flexible simulation tool for particle-based materials modeling at the atomic, meso, and continuum scales. *Comput. Phys. Commun.* **2022**, *271*, 108171.

https://doi.org/10.1021/acs.jpclett.6c01096
J. Phys. Chem. Lett. 2026, 17, 6357−6364